




Evaluation of the structural and magnetic properties of $\text{Sr}_4\text{Fe}_6\text{O}_{13}$ ceramics prepared from nanoplatelets of $\alpha\text{-Fe}_2\text{O}_3$

Harikrishnan Vijayan^{1,6,*} , Gomathi Ramasamy², Ramki Chakaravarthy³, Ganesamoorthy Ramasamy⁴, and K. S. Syam Kishor⁵

¹ Department of Chemistry, Aarhus University, Langelandsgade 140, 8000 Aarhus C, Denmark

² Department of Physics, Allied Health Sciences, Dr. MGR Educational & Research Institute, Chennai 600077, India

³ Department of Physics, Dr. M. G. R. Educational and Research Institute University, Arni 632317, India

⁴ Department of Chemistry, Vinayaka Mission's Kirupananda Variyar Arts and Science College, Salem, Tamil Nadu 636 308, India

⁵ Government College Ambalapuzha, Alappuzha 688561, Kerala, India

⁶ IMDEA-Nanociencia, Campus Universidad Autonoma de Madrid, 28049 Madrid, Spain

Received: 7 June 2025

Accepted: 27 September 2025

Published online:

17 October 2025

© The Author(s), under exclusive licence to Springer Science+Business Media, LLC, part of Springer Nature, 2025

ABSTRACT

$\text{Sr}_4\text{Fe}_6\text{O}_{13}$ phases were prepared by employing nanoplatelets of $\alpha\text{-Fe}_2\text{O}_3$ with appreciable magnetic properties. This is novel work based on the synthesis strategy of $\text{Sr}_4\text{Fe}_6\text{O}_{13}$, where we have employed both the hydrothermal synthesis and subsequent annealing, followed by solid-state mixing. We have employed hydrothermal synthesis, and subsequent annealing of powders resulted in the formation of $\alpha\text{-Fe}_2\text{O}_3$ with platelet morphology, with average particle sizes of 81(2) nm. These platelets were mixed with SrCO_3 and annealed at three different temperatures of 900 °C, 1000 °C, and 1100 °C. This synthesis strategy resulted in the highest coercivity of 343 kA/m at 1000 °C. An appreciable saturation magnetization of 21 Am^2/kg was obtained for the powders annealed at 1100 °C. The Rietveld modeling of the powder diffraction patterns of $\text{Sr}_4\text{Fe}_6\text{O}_{13}$ annealed at different temperatures showed the presence of impurity phases in all the three temperatures; however, the powder annealed at 1100 °C showed highest amount of $\text{Sr}_4\text{Fe}_6\text{O}_{13}$ with 87%. The results confirm that there is influence of $\text{SrFe}_{12}\text{O}_{19}$ on the formation of $\text{Sr}_4\text{Fe}_6\text{O}_{13}$ phase.

1 Introduction

The $\text{SrO-Fe}_2\text{O}_3$ is considered to be a pseudo binary phase which consists of lot of intermediary phases. In this system, we have layered perovskite structure based on $\text{Sr}_4\text{Fe}_6\text{O}_{13}$ compounds [1]. The crystal

structure of $\text{Sr}_4\text{Fe}_6\text{O}_{13}$ was prepared for the first time by Kanamaru et al. [2]. It was also shown by Yoshiasa et al. that a stable phase of about 42 mol % Fe_2O_3 is required in order to obtain $\text{Sr}_4\text{Fe}_6\text{O}_{13}$ [3]. This perovskite-related material has earned a lot of attention as possible candidate for oxygen separation membranes

Address correspondence to E-mail: getharikrishnan@gmail.com; vijayan.harikrishnan@imdea.org

[4]. Its precise crystal structure description led to the detection of structural incommensurability [5]. This phase was also reinvestigated for the Sr-rich part of the SrO–Fe₂O₃ system by Fossdal et al. [6]. A Sr–Fe–O system includes many types of perovskites and perovskite derivatives of widely varied crystalline and magnetic features [7]. The basic building block involved in the construction of Sr₄Fe₆O₁₃ has a perovskite and its derivatives. There are also non-perovskite layers which are present in the structure because of the O²⁻ non stoichiometry, and due to this reason, the structure is often represented as Sr₄Fe₆O_{13-δ} [8–12]. These mixed conducting oxides have high oxygen conductivity and electronic conductivity because they hold great promise for industrial use as oxygen separation membrane from selective oxidation of hydrocarbons and electrodes in solid oxide fuel cells [13].

The common synthesis route followed in order to obtain Sr₄Fe₆O₁₃ is a solid-state sintering route. Apart from this, Rossel et al. had reported the thin film deposition of Sr₄Fe₆O₁₃ on substrates like SrTiO₃ [13]. Azab et al. had reported the synthesis of Sr₄Fe₆O₁₃ employing citrate auto-combustion method [8]. They had investigated the particles for their morphology, magnetic, and dielectric properties. This study is relevant to the present study in terms of the magnetic properties, where they obtained a maximum coercivity, H_C of 336 kA/m, and saturation magnetization M_S of 22.8 Am²/kg. Apart from this, they had also investigated the particles at different temperatures. Hongliang Luo had reported the synthesis of Sr₄Fe₆O₁₃ employing a traditional solid-state milling process, where oxides were ball-milled and followed by sintering the particles at 1100 °C/2 h [14]. However, they had investigated only the microwave absorption properties of the particles. The X-ray diffraction pattern of the powders relatively displayed a pure phase of Sr₄Fe₆O₁₃ and is comparable to the present study. Another study from Min Feng Lu et al. reported the reduction of Sr₄Fe₆O₁₃ to Sr₄Fe₆O₁₂ with an average oxidation state of Fe^{2.667+} [15]. The synthesis of Sr₄Fe₆O₁₂ involved the topotactic reduction, which resulted in a unique pair of edge-linked Fe^{2.5+}O₄ tetrahedra at 300 K. The Sr₄Fe₆O₁₃ particles were synthesized by solid-state synthesis and subsequently reduced to Sr₄Fe₆O₁₂. Shanshan Jiang et al. had synthesized Sr₄Fe₆O₁₃ using the ethylenediaminetetraacetic acid (EDTA)–citrate complex route [16]. The particles were annealed at 1050 °C/2 h and studied for their structural stability through in situ X-ray diffraction from room temperature to 1050 °C with 10 °C/

min. The exploitation of the morphology of precursors has been previously reported in the case of SrFe₁₂O₁₉ magnets [17–21]. The reports were largely based on employing the non-ferromagnetic precursors for making SrFe₁₂O₁₉ magnets. The major advantage of this method was to exploit the non-interacting grains of precursors while converting to the hexaferrite phase. Another major advantage of this method was that the conversion was possible at relatively lower annealing temperature. Along these lines, the present study aims to make Sr₄Fe₆O₁₃ particles with higher coercivity H_C and respectable saturation magnetization M_S employing non-ferromagnetic precursors, which in this case are the platelets of hematite nanoparticles. However, it has to be noted that Sr₄Fe₆O₁₃ is antiferromagnetic in nature [22]. We have employed a combination of both solid-state and hydrothermal synthesis routes to make Sr₄Fe₆O₁₃ particles. This type of combination of two synthesis routes has not been performed in the literature. The basic purpose of adapting the hydrothermal synthesis method in this particular work was to obtain the platelets of hematite nanoparticles. We also want to observe the influence of the morphology of hematite (α-Fe₂O₃) nanoparticles on making the final strontium ferrite (Sr₄Fe₆O₁₃). All the previous reports mentioned in the manuscript were concentrating on solid-state methods to obtain; however, in the present work, we concentrated more on the influence of the morphology of these hematite platelets in obtaining perovskite-based strontium ferrite. Initially, we have made platelets of hematite nanoparticles in the presence of a cationic surfactant called Cetyltrimethylammonium bromide (CTAB) and then added SrCO₃, which were subsequently annealed at 900, 1000, and 1100 °C/1 h. We have employed X-ray diffraction along with Rietveld analysis to understand the structure of Sr₄Fe₆O₁₃ particles. The evolution of magnetic properties at different temperatures has also been investigated in the present work. Figure 1 represents the three important processes involved in making Sr₄Fe₆O₁₃ phase.

2 Experimental section

2.1 Preparation of α-Fe₂O₃, hematite nanoparticles

The hematite nanoparticles were prepared by a combination of hydrothermal synthesis and subsequent annealing of resultant powders at 700 °C/2 h.

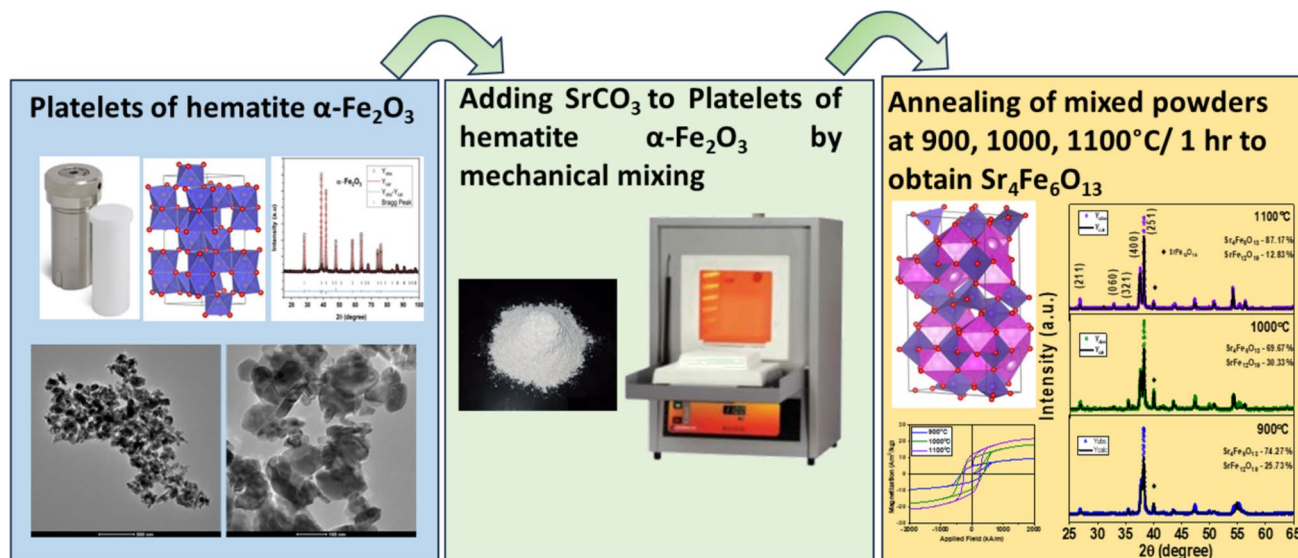


Fig. 1 Schematic representing the overall process involved in making $\text{Sr}_4\text{Fe}_6\text{O}_{13}$ phase

Initially, a 1 M solution of $\text{Fe}(\text{NO}_3)_3 \cdot 9\text{H}_2\text{O}$ was prepared, and toward it, an 8.0 M solution of NaOH was added dropwise under constant magnetic stirring, causing a transparent red solution to form a gel-like compound. The $[\text{OH}^-]/[\text{NO}_3^-]$ ratio was 1.11. A cationic surfactant, Cetyl trimethyl ammonium bromide (CTAB) with 1 wt. % was added to the solution. Then, toward the end, the precursor gel was transferred to a 175 ml autoclave and placed inside an oven for 15 h at 200 °C. The resultant was washed several times with deionized water to remove impurities. The resultant solution was dried at 80 °C overnight in an oven and then ground to obtain powders. The details of it are discussed further in Sect. 3.

2.2 Preparation of $\text{Sr}_4\text{Fe}_6\text{O}_{13}$ particles

The $\alpha\text{-Fe}_2\text{O}_3$, hematite nanoparticles were mixed together with SrCO_3 to obtain $\text{Sr}_4\text{Fe}_6\text{O}_{13}$. The ratio of Fe/Sr was adjusted to 3 by the addition of SrCO_3 to get 1 g of the mixture of SrCO_3 and $\alpha\text{-Fe}_2\text{O}_3$. The resultant mixture was annealed at 900 °C, 1000 °C, and 1100 °C for 1 h.

2.3 Characterization

2.3.1 Thermogravimetry and differential scanning calorimetry

Thermogravimetry and differential scanning calorimetry of the as-prepared powders were performed using

the NETZCH DSC 404 F1 Pegasus instrument. 10 mg of the powders was loaded into an alumina crucible, and data were recorded from 80 °C to 650 °C at a heating rate of 5 °C/min.

2.3.2 Powder X-ray diffraction

The diffraction patterns of the hematite nanoparticles annealed at 700 °C and strontium ferrite $\text{Sr}_4\text{Fe}_6\text{O}_{13}$ were collected using a Rigaku Smart Lab diffractometer, Rigaku Japan equipped with a Co source and a D/teX Ultra detector. Rietveld refinements were carried out in Fullprof [23] on all the powder X-ray diffraction (PXRD) patterns using the Thomas-Cox-Hastings pseudo-Voigt function to describe the peak profile of the diffraction pattern. We have refined the zero-point correction, scale factor, and lattice constants. The Lorentzian anisotropic crystallite size parameter γ was refined for both $\alpha\text{-Fe}_2\text{O}_3$ and $\text{Sr}_4\text{Fe}_6\text{O}_{13}$. The preferred orientation S_z was not refined for both $\alpha\text{-Fe}_2\text{O}_3$ and $\text{Sr}_4\text{Fe}_6\text{O}_{13}$ phases. The instrumental peak broadening was obtained by measuring a NIST LaB6 660B standard under identical instrument conditions.

2.3.3 Transmission electron microscopy

Transmission electron microscopy and elemental analysis were recorded on an FEI TALOS F200A (200 kV)

(S)TEM microscope for the $\alpha\text{-Fe}_2\text{O}_3$, which was made at 700 °C, and $\text{Sr}_4\text{Fe}_6\text{O}_{13}$ particles annealed at 1100 °C.

2.3.4 Magnetic properties

The magnetic properties of the powder samples were measured with a Quantum Design, Physical Property Measurement System equipped with a vibrating sample magnetometer (VSM).

3 Results

3.1 Thermogravimetric analysis and differential scanning calorimetry analysis

The thermogravimetry analysis (TGA) along with differential scanning calorimetry (DSC) curves of the as-prepared hydrothermally synthesized powders and dried at 80 °C is shown in Fig. 2. The TGA curve shows a weight loss between 100 °C and 150 °C. This may be attributed to the removal of the surface water molecules. The next major weight loss is observed between 200 °C and 300 °C. This may be attributed to two reasons. The first one may be due to the decomposition of CTAB [24], and the second may be due to phase transition to hematite as this is also accompanied by the endothermic peak in the DSC curve as seen from Fig. 2. The annealing temperature of the as-prepared hydrothermal powders was decided to be 700 °C/2 h

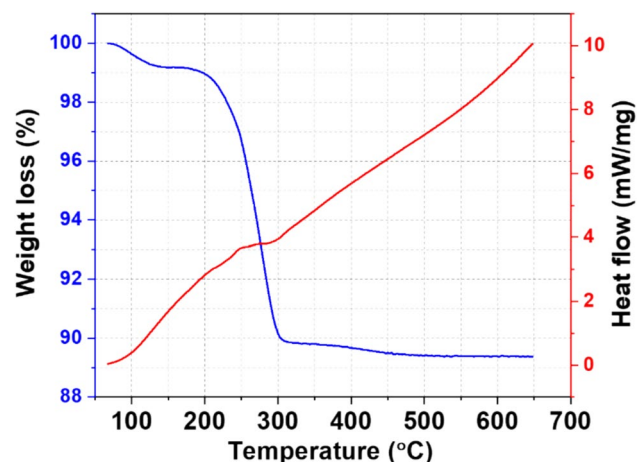


Fig. 2 Thermogravimetry analysis and differential scanning calorimetry plot for the as-prepared hydrothermal synthesized mixture containing both hematite and goethite nanoparticles

because the main aim was to obtain platelet morphology of the powders which would be subjected to conversion to $\text{Sr}_4\text{Fe}_6\text{O}_{13}$ with the addition of SrCO_3 .

3.2 X-ray diffraction analysis of hematite nanoparticles

The powder diffraction pattern and corresponding Rietveld refinement for the hematite is shown in Fig. 3 revealing a phase-pure sample. The hematite phase crystallized in the rhombohedral structure with R-3C space group. The lattice parameters extracted from refinement of the sample were $a = b = 5.03458(2)$ Å, $c = 13.74592(6)$ Å. The crystallite size extracted from X-ray diffraction patterns was found to be 63 nm. It has to be noted that the as-prepared hydrothermal synthesized powder was annealed at 700 °C/2 h. The morphology of the hematite nanoparticles corresponds to platelet morphology which is further discussed in Sect. 3.4.

3.3 X-ray diffraction analysis $\text{Sr}_4\text{Fe}_6\text{O}_{13}$ nanoparticles annealed at 900 °C, 1000 °C, and 1100 °C

For further processing the $\text{Sr}_4\text{Fe}_6\text{O}_{13}$ structure, the hematite $\alpha\text{-Fe}_2\text{O}_3$ was mixed with SrCO_3 and subjected to annealing at 900 °C, 1000 °C and 1100 °C for an hour. The Rietveld refined X-ray diffraction

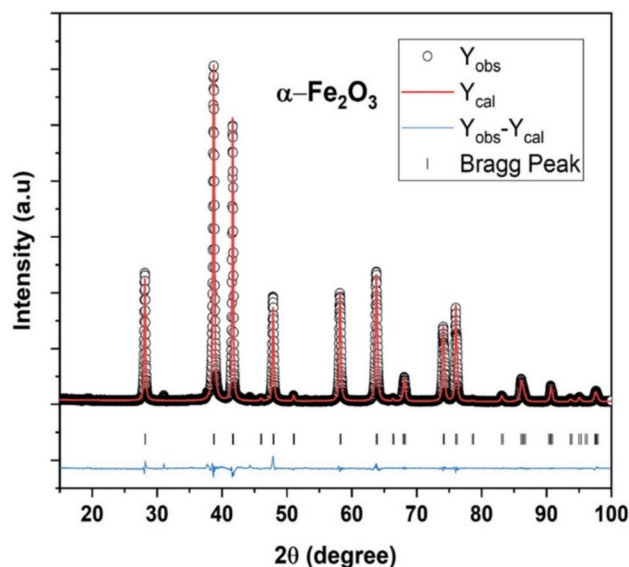


Fig. 3 The X-ray diffraction pattern and Rietveld refinement of hematite nanoparticles along with the Bragg reflections at 700 °C/2 h

patterns of the annealed $\text{Sr}_4\text{Fe}_6\text{O}_{13}$ nanoparticles are shown in Fig. 4. The X-ray diffraction pattern showed the presence of the impurity phase of Strontium hexaferrite ($\text{SrFe}_{12}\text{O}_{19}$). The weight fractions of the phases extracted from the refinement of the samples annealed at three different temperatures are shown in Fig. 4. The highest purity of the sample was found at 1100 °C with 87.17% of $\text{Sr}_4\text{Fe}_6\text{O}_{13}$; however for 1000 °C, the highest amount of $\text{SrFe}_{12}\text{O}_{19}$ was found with 30.33%. There is a previous report on the synthesis temperature for $\text{Sr}_4\text{Fe}_6\text{O}_{13}$, which has been 1100 °C [1, 4–8, 14, 25–27]. The same synthesis temperature has been employed in the present work where we get the highest purity samples at 1100 °C. The synthesis temperature also influences the magnetic properties of the samples. This is further discussed in Sect. 3.5. The lattice parameters extracted from the refinement of the samples are shown in Table 2. The annealing process of the hematite and strontium mixture converts to $\text{Sr}_4\text{Fe}_6\text{O}_{13}$. The rhombohedral structure of $\alpha\text{-Fe}_2\text{O}_3$ transforms into the orthorhombic structure of $\text{Sr}_4\text{Fe}_6\text{O}_{13}$. The lattice constants for $\text{Sr}_4\text{Fe}_6\text{O}_{13}$ annealed

at different temperatures are shown in Table 2. It is to be noted that the lattice constant a and b varies largely for the powders annealed at 900, 1000, and 1100 °C. The b -axis is considered to be the long axis in the case of the $\text{Sr}_4\text{Fe}_6\text{O}_{13}$ structure. The values extracted from the Rietveld refinement, along with the volume and Wyckoff positions for $\text{Sr}_4\text{Fe}_6\text{O}_{13}$ and $\text{SrFe}_{12}\text{O}_{19}$, are displayed in Table 1(a) and (b). The details regarding the structure and conversion are discussed in the discussion section.

3.4 Transmission electron micrographs of hematite and perovskite strontium ferrite

The Transmission electron micrograph of the hematite $\alpha\text{-Fe}_2\text{O}_3$ with particle size distribution and perovskite-type $\text{Sr}_4\text{Fe}_6\text{O}_{13}$ is shown in Fig. 5(a) – (f). The $\alpha\text{-Fe}_2\text{O}_3$ nanoparticles show the presence of irregular platelet-like morphology with broad particle size distribution revealing the approximate particle size to be 81(2) nm. The strontium precursor is then added to the hematite mixture by mechanical mixture, and the resultant mixture was subjected to annealing at different temperatures of 900, 1000, and 1100 °C. There is abnormal aggregation of Sr^{2+} ions observed in the elemental mapping that may be attributed to the inhomogeneous distribution while grinding the SrCO_3 to the $\alpha\text{-Fe}_2\text{O}_3$ nanoparticles.

3.5 Magnetic properties of $\text{Sr}_4\text{Fe}_6\text{O}_{13}$ annealed at 900 °C, 1000 °C, and 1100 °C

Figure 6(a) depicts the magnetic hysteresis loops of samples made from hematite ($\alpha\text{-Fe}_2\text{O}_3$) precursors and SrCO_3 at different annealing temperatures of 900 °C, 1000 °C, and 1100 °C. Table 2 represents the details about the magnetic properties such as the saturation magnetization, (M_s), remanent magnetization (M_R), and coercivity, (H_C) of the samples. The description of the variation of each magnetic property has been discussed in detail below.

3.5.1 Saturation magnetization, M_S

The perovskite $\text{Sr}_4\text{Fe}_6\text{O}_{13}$ is an inherently antiferromagnetic in nature as has been reported elsewhere [22]. From the hysteresis loop, it can be confirmed that the samples show ferromagnetic nature. This may be partly

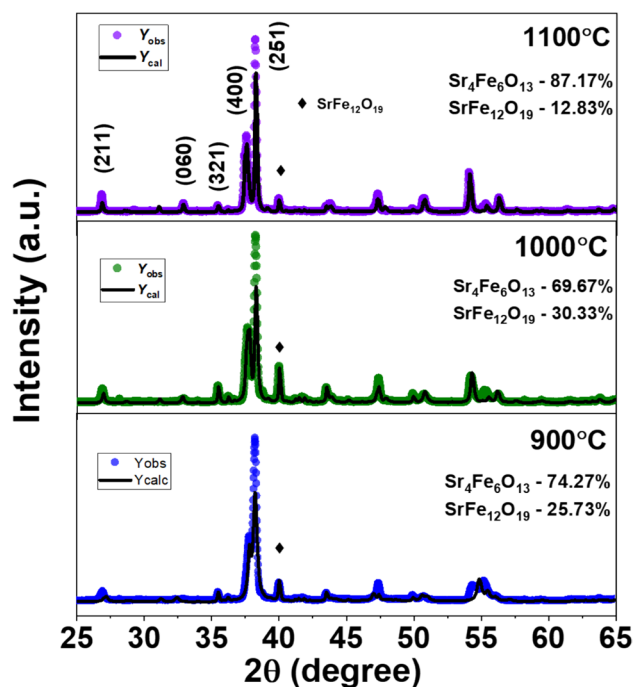


Fig. 4 a–c X-ray diffraction pattern and Rietveld refinement of the powder samples annealed at 900 °C, 1000 °C, and 1100 °C/1 h. The black lines represent the Rietveld model (Y_{cal}), while blue, green, and violet circles represent the observed X-ray diffraction pattern (Y_{obs}). The weight fractions of samples extracted from Rietveld refinement are also indicated in the figure

Table 1 (a) & (b) Space group and atomic positions and volume of two phases employed in the refinement of X-ray diffraction pattern comprising perovskite-based Strontium ferrite(Sr₄Fe₆O₁₃) structure along with the impurity phase of hexagonal strontium ferrite (SrFe₁₂O₁₉)

Crystal System			Orthorhombic
<i>Space group</i>			<i>Iba2</i>
<i>Atom Parameters</i>	x/a	y/b	z/c
<i>Sr 1</i>	0.36480	0.34320	0.00200
<i>Sr 2</i>	0.38050	0.16260	0.00000
<i>Fe 1</i>	0.12470	0.04010	0.04300
<i>Fe 2</i>	0.11410	0.45630	0.08000
<i>Fe 3</i>	0.12000	0.24420	−0.00400
<i>O1</i>	0.14100	0.13500	−0.03000
<i>O2</i>	0.12600	0.36500	−0.02000
<i>O3</i>	−0.00800	0.24200	0.24000
<i>O4</i>	0.25100	0.25000	0.26000
<i>O5</i>	0.21100	0.03900	0.38000
<i>O6</i>	0.41100	0.03900	−0.07000
<i>O7</i>	0.50000	0.50000	−0.19000
χ^2			18
R_{wp}			24.9
Volume, V (Å ³)			1173.8(5)
Crystal System			Hexagonal
<i>Space group</i>			<i>P63/mmc</i>
<i>Atom Parameters</i>	x/a	y/b	z/c
<i>Sr 1</i>	0.33333	0.66667	0.75000
<i>Fe 1</i>	0.00000	0.00000	0.00000
<i>Fe 2</i>	0.00000	0.00000	0.25805
<i>Fe 3</i>	0.33333	0.66667	0.02785
<i>Fe 4</i>	0.33333	0.66667	0.19053
<i>Fe 5</i>	0.16833	0.33670	−0.10969
<i>O1</i>	0.00000	0.00000	0.15160
<i>O2</i>	0.33333	0.66667	−0.05520
<i>O3</i>	0.18280	0.36560	0.25000
<i>O4</i>	0.15630	0.31260	0.05240
<i>O5</i>	0.50510	0.01020	0.15100
Volume, V (Å ³)			688.5 (4)

attributed to the fact that there is presence of impurity phase of SrFe₁₂O₁₉. This is concluded from the X-ray diffraction studies as well. The sample annealed at 1000 °C shows the presence of maximum impurity phase of 30% of SrFe₁₂O₁₉. The highest saturation magnetization M_s was seen at 1100 °C. This may be partly attributed to the presence of SrFe₁₂O₁₉. However, Azab et al. have reported a maximum M_s of 22.2 Am²/kg which is closer to the report of the present work [8]. They had annealed the sample at 1100 °C/3 h. The magnetic moment of

SrFe₁₂O₁₉ arises from the different sublattices of Fe. There are five different sublattices of Fe mainly octahedral (2a, 4f₂, 12 k), bipyramidal (2b), and tetrahedral (4f₁). The easy axis of strontium hexaferrite is considered to be along the c-axis. As already discussed in the introduction section, Sr₄Fe₆O₁₃ has a construction of a perovskite or its derivatives. It consists of dual slabs of FeO in FeO₄/FeO₅ polygon. The double-layer polyhedra are highly distorted with the geometry of the four coordinated sites described alternatively as distorted

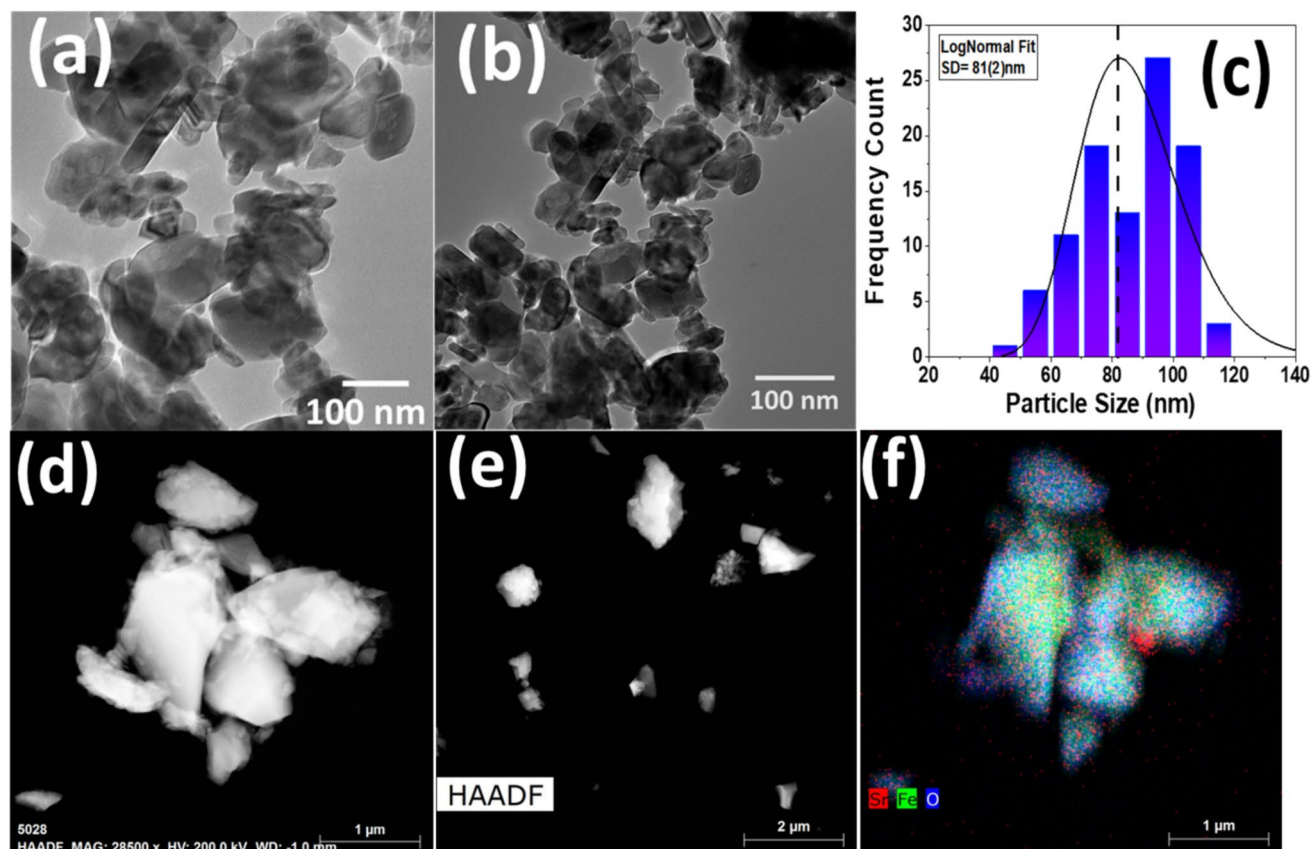


Fig. 5 a, b Transmission electron micrograph of the α -Fe₂O₃ nanoplatelets & c particle size distribution of hematite d–f the HAADF image of sample annealed at 1100 °C/1 h

Fig. 6 Hysteresis of annealed powder samples of Sr₄Fe₆O₁₃. The maximum H_C of the sample is observed at 1000 °C although there is not much difference between the H_C of 900 °C and 1000 °C sample however the saturation magnetization M_S is seen to have large variation. The details of the variation can be found in Sect. 3.3

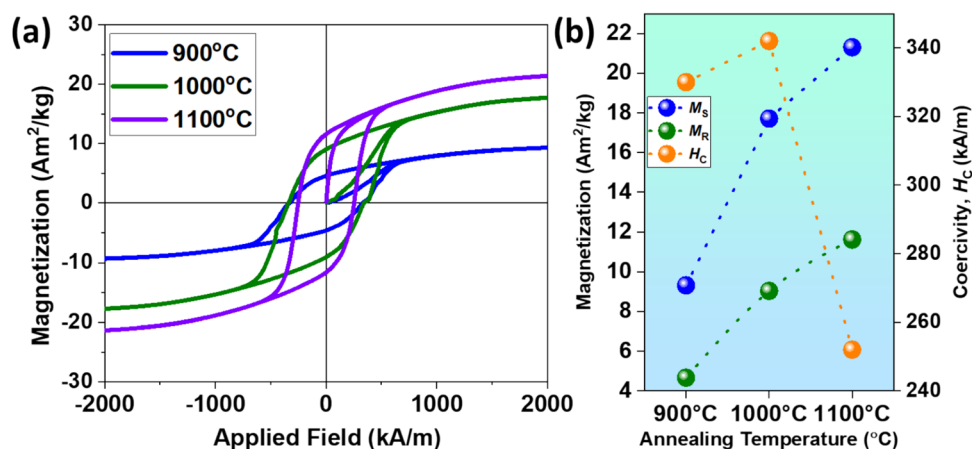


Table 2 Lattice constants and magnetic properties extracted from the X-ray diffraction and hysteresis of the nanoparticles

Annealing temperature	Lattice Constants of Sr ₄ Fe ₆ O ₁₃			Saturation Magnetization, M_S (Am ² /kg)	Remanence Magnetization, M_R (Am ² /kg)	Coercivity, H_C (kA/m)
	a (Å)	b (Å)	c (Å)			
900 °C	10.923(2)	19.239(2)	5.527(3)	9.32	4.66	330
1000 °C	11.085(3)	19.018(3)	5.562(2)	17.71	9.04	342
1100 °C	11.102(3)	18.966(3)	5.573(2)	21.31	11.62	252

tetrahedral. As far $\text{Sr}_4\text{Fe}_6\text{O}_{13}$ is concerned, it consists of three different sublattices of Fe ions. It is reported that the structure is antiferromagnetic in nature [22]. The hysteresis at 900 °C and 1000 °C displays domain wall motion, while at 1100 °C displays nucleation wall pinning motion [28].

3.5.2 Coercivity, H_C

The H_C of the sample annealed at 900, 1000, and 1100 °C is shown in Fig. 4(b). The coercivity H_C of 900 and 1000 °C samples is almost comparable, while there is a sharp decrease in the case of 1100 °C. This may be attributed to the decrease of coercivity with increasing annealing temperature, which is usually seen in the case of nanoparticles due to the transition from single domain region to multiple domain region. However, in the present report, we have obtained higher values of coercivity H_C when compared with previous report of Azab et al. [8]. This study reports better coercivity values when compared with the previously reported values [8, 29].

4 Discussion

The present work sheds light on the synthesis of $\text{Sr}_4\text{Fe}_6\text{O}_{13}$ perovskite structure with the help of hematite platelets. There are several synthesis routes for the preparation of this perovskite structure reported in the literature as discussed earlier; however, this is the first time where the hydrothermally synthesized platelets of $\alpha\text{-Fe}_2\text{O}_3$ have been employed to prepare the $\text{Sr}_4\text{Fe}_6\text{O}_{13}$ nanoparticles. The powders of hematite were then mixed with a Strontium source of SrCO_3 in excess. The resultant mixture was then annealed at high temperatures of 900, 1000, and 1100 °C for one hour. We were able to successfully make the perovskite structure of $\text{Sr}_4\text{Fe}_6\text{O}_{13}$ as the results from the X-ray diffraction have already been discussed. The important part of understanding the conversion of $\text{Sr-Fe}_2\text{O}_3$ to $\text{Sr}_4\text{Fe}_6\text{O}_{13}$ is to closely analyze the structure of both. They are explained in the next sections.

4.1 Correlation between hematite ($\alpha\text{-Fe}_2\text{O}_3$) and perovskite-based strontium ferrite ($\text{Sr}_4\text{Fe}_6\text{O}_{13}$)

There are various reports available on the rhombohedral structure of hematite. The usual morphology of

hematite is in the form of platelets as reported in this work. As far as the correlation is concerned, Langhof et al. have reported the influence of Fe-rich phase as part of the $\text{SrO-Fe}_2\text{O}_3$ structural system [7]. They have reported the existence of $\text{Sr}_4\text{Fe}_6\text{O}_{13}$ along with M-Type strontium hexaferrite $\text{SrFe}_{12}\text{O}_{19}$ at $T > 1150$ °C. They have observed the existence of $\text{Sr}_4\text{Fe}_6\text{O}_{13}$ along with the perovskite structure of SrFeO_3 above 1150 °C until 1250 °C. However, in the present work, we have reported the existence of $\text{Sr}_4\text{Fe}_6\text{O}_{13}$ along with the M-Type hexaferrite $\text{SrFe}_{12}\text{O}_{19}$ at 1100 °C, taking into account the error in the furnaces we have employed in annealing the powders compared with that of the literature. It has to be noted that we have not included the influence of oxygen vacancies in the present work. The structure is usually reported as $\text{Sr}_4\text{Fe}_6\text{O}_{13-\delta}$; however, we have not reported the existence of δ in the present work as we do not have enough characteristic evidence to report the same. However, in the present report, we have shed light on the lower synthesis temperature of $\text{Sr}_4\text{Fe}_6\text{O}_{13}$ as the annealing temperature employed in the present report ranges from 900 °C to 1100 °C. According to Fossdal et al., calcinating the powders below 775 °C resulted in the formation of SrFeO_3 and $\text{SrFe}_{12}\text{O}_{19}$. The $\text{Sr}_4\text{Fe}_6\text{O}_{13}$ was only formed while calcinating the powders above 775 °C [6]. They also report the stability of $\text{Sr}_4\text{Fe}_6\text{O}_{13}$ in the context of Fe_2O_3 concentration. The $\text{Sr}_4\text{Fe}_6\text{O}_{13}$ is found to be stable between 775 °C and 1150 °C which was depicted with the help of the phase diagram reported by Fossdal et al. The above comparison was performed in the context of calcination temperature and the concentration of $\text{Sr}_4\text{Fe}_6\text{O}_{13}$; however, there should be a comparison based on the structure.

In the present work, the synthesis of hematite is performed by employing hydrothermal synthesis in the presence of a cationic surfactant known as cetyl trimethyl ammonium bromide (CTAB). The as-prepared powders were subjected to calcination at 700 °C/2 h to complete the phase transition in order to obtain the morphology of platelets of hematite. Figure 7 shows the comparison of the structures that are discussed in the present manuscript. As shown in the figure, the hematite crystallizes in the space group of R-3C with rhombohedral symmetry with a long C axis, while perovskite-based $\text{Sr}_4\text{Fe}_6\text{O}_{13}$ crystallizes in the orthorhombic structure with the Iba2 space group. The number of atoms in a conventional unit cell of $\text{Sr}_4\text{Fe}_6\text{O}_{13}$ is 16:24:52 with (Sr:Fe:O). The structure is built up of alternating layers of perovskite-type

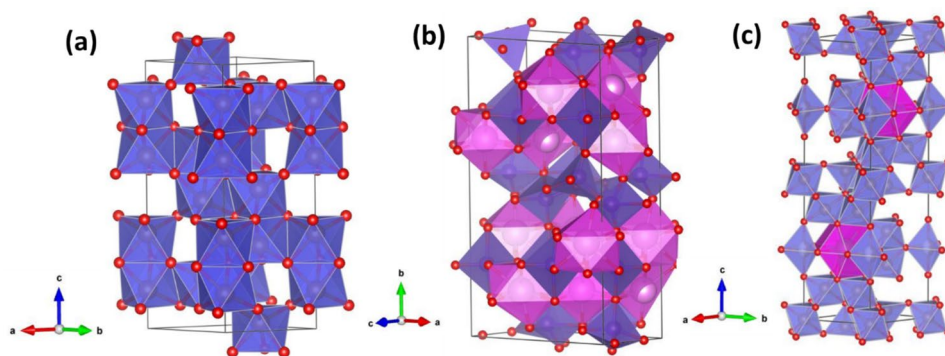


Fig. 7 The vesta software generated figure shows the structure of **a** hematite ($\alpha\text{-Fe}_2\text{O}_3$) rhombohedral R-3C with $a=b=5.03458(2)$ Å, $c=13.74592(6)$ Å & **b** perovskite-based strontium ferrite $\text{Sr}_4\text{Fe}_6\text{O}_{13}$, the oxide possesses orthorhombic structure with Iba2 space group with $a=11.103$ Å, $b=18.924$ Å, $c=5.572$ Å **c** the

lattice structure of $\text{SrFe}_{12}\text{O}_{19}$ which forms as part of an impurity phase is also shown in the figure for comparison purposes. The long axis in the case hematite ($\alpha\text{-Fe}_2\text{O}_3$) and strontium hexaferrite ($\text{SrFe}_{12}\text{O}_{19}$) is the c-axis; however, in the case of perovskite strontium ferrite $\text{Sr}_4\text{Fe}_6\text{O}_{13}$, it is the b-axis as shown in the figure

octahedra with mixed $\text{FeO}_4/\text{FeO}_5$ polyhedra with a long axis along b . The structure of hematite consists only of octahedral coordination of Fe^{3+} ions. Mathias et al. had made an attempt to compare the structures of $\alpha\text{-Fe}_2\text{O}_3$ and $\text{SrFe}_{12}\text{O}_{19}$ [21]. They have explained the transformation from goethite to hematite to strontium hexaferrite reaction in the form of topotactic pseudomorphic phase transition. With the present results it is not possible to conclude a similar topotactic pseudomorphic phase transition for hematite to strontium ferrite. It has to be noted that controlling the impurities is difficult while making $\text{Sr}_4\text{Fe}_6\text{O}_{13}$ samples. The main aim of the present work was to show that the platelets of hematite can be employed to make $\text{Sr}_4\text{Fe}_6\text{O}_{13}$. We speculate that there is a contribution of impurity phase of $\text{SrFe}_{12}\text{O}_{19}$ toward the magnetic properties at 1000 °C. However, we are in the process of improving the phase purity of $\text{Sr}_4\text{Fe}_6\text{O}_{13}$ and would include it in our next work. Bardal et al. have reported about the presence of $\text{SrFe}_{12}\text{O}_{19}$ while preparing La-doped $\text{Sr}_4\text{Fe}_6\text{O}_{13}$ samples [30].

5 Conclusion

We were able to demonstrate for the first time a new strategy to make $\text{Sr}_4\text{Fe}_6\text{O}_{13}$ from platelets of $\alpha\text{-Fe}_2\text{O}_3$. The platelets of $\alpha\text{-Fe}_2\text{O}_3$ were prepared by hydrothermal synthesis technique in the presence of cationic surfactant and followed by annealing of the powders at 700 °C/2 h. The resultant precursor powders were mixed with SrCO_3 and annealed at 900 °C,

1000 °C, and 1100 °C. The Rietveld refinement of the X-ray powder diffraction reveals the presence of the $\text{Sr}_4\text{Fe}_6\text{O}_{13}$ highest at 1100 °C. However, the coercivity of the powder was found to be highest at 1000 °C with 343 kA/m mainly because of the presence of $\text{SrFe}_{12}\text{O}_{19}$ impurity phase. A respectable saturation magnetization M_s for $\text{Sr}_4\text{Fe}_6\text{O}_{13}$ was seen at 1100 °C with 21 Am²/kg enhancing the ferromagnetic nature. The partial contribution of M_s may be attributed to the presence of $\text{SrFe}_{12}\text{O}_{19}$ in the phase. The synthesis strategy of making $\text{Sr}_4\text{Fe}_6\text{O}_{13}$ will pave the way in the future to make this structure with maximum purity for oxide interfaces in oxide heterojunctions to accommodate charge transfer, non-linear optics, and exchange.

Acknowledgements

One of the authors, Harikrishnan, would like to thank the Innovation Fund Denmark for the grant in the Innoexplorer program (GCAM 1046-00025B).

Author contributions

Investigation, formal analysis, writing and reviewing, funding acquisition, and project administration: Harikrishnan Vijayan; writing and reviewing: Gomathi Ramasamy; reviewing: Ramki Chakaravathy; reviewing: Ganesamoorthy Ramasamy; writing and reviewing: S Syam Kishor.

Funding

Innovationsfonden, GCAM 1046-00025B, Harikrishnan Vijayan.

Data availability

The authors declare that the data supporting the findings of this study are available within the paper.

Declarations

Conflict of interest The authors declare that they have no conflicts of interest.

Ethical approval The authors declare that this manuscript complies with scientific ethical standards. Furthermore, this article does not contain any studies involving human or animal participants.

References

1. M.Y. Avdeev, M.V. Patrakeeve, V.V. Kharton, J.R. Frade, J. Solid State Electrochem. **6**, 217 (2002)
2. Journal of Physics and Chemistry of Solids **33**, 1169 (1972).
3. A. Yoshiasa, K. Ueno, F. Kanamaru, H. Horiuchi, Mater. Res. Bull. **21**, 175 (1986)
4. R. Bredesen, T. Norby, A. Bardal, V. Lynam, Solid State Ion. **135**, 687 (2000)
5. B. Mellenne, R. Retoux, C. Lepoittevin, M. Hervieu, B. Raveau, Chem. Mater. **16**(24), 5006–5013 (2004)
6. A. Fossdal, M.A. Einarsrud, T. Grande, J. Solid State Chem. **177**, 2933 (2004)
7. N. Langhof, D. Seifert, M. Göbbels, J. Töpfer, J. Solid State Chem. **182**, 2409 (2009)
8. A.A. Azab, A.M. Mansour, G.M. Turkey, Sci. Rep. **10**, 1 (2020)
9. C.A.J. Fisher, M.S. Islam, J. Mater. Chem. **15**, 3200 (2005)
10. S.P. Badwal, F.T. Ciacchi, Adv. Mater. **13**(12–13), 993–996 (2001)
11. J.C. Waerenborgh, M. Avdeev, M.V. Patrakeeve, V.V. Kharton, J.R. Frade, Mater. Lett. **57**, 3245 (2003)
12. J.A. Kilner, Solid State Ion. **129**, 13 (2000)
13. M.D. Rossell, A.M. Abakumov, G. Van Tendeloo, J.A. Pardo, J. Santiso, Chem. Mater. **16**, 2578 (2004)
14. H. Luo, H. Hao, Q. Guo, M. Cao, Z. Yao, H. Liu, J. Mater. Sci. Mater. Electron. **33**, 14672 (2022)
15. M.F. Lü, J.C. Waerenborgh, C. Greaves, Angewandte Chemie - International Edition **52**, 4833 (2013)
16. S. Jiang, W. Zhou, J. Sunarso, R. Ran, Z. Shao, Int. J. Hydrogen Energy **40**, 15578 (2015)
17. H. Vijayan, C.G. Knudsen, M.I. Mørch, M. Christensen, Mater. Chem. Front. (2021). <https://doi.org/10.1039/D1QM00224D>
18. H. Vijayan, A.P. Laursen, M. Stingaciu, P. Shyam, F.H. Gjørup, J. Simonsen, M. Christensen, ACS Appl. Nano Mater. **6**, 8156 (2023)
19. J. Thomas-hunt, A. Povlsen, H. Vijayan, C.G. Knudsen, F.H. Gjørup, M. Christensen, Dalton Trans. **51**, 3884 (2022)
20. H. Vijayan, A. Povlsen, J. Thomas-Hunt, M.I. Mørch, M. Christensen, J. Alloys Compd. **915**, 165333 (2022)
21. M.I. Mørch, J. Thomas-Hunt, A.P. Laursen, J. Simonsen, J.P. Frandsen, H. Vijayan, M. Christensen, Chem. Mater. **36**, 1919 (2024)
22. S. Huang, K. Zhu, J. Huang, J. Yang, J. Wang, Z. Fu, R. Peng, Y. Lu, Ceram. Int. **48**, 19963 (2022)
23. J. Rodriguez-Carvajal, Phys. B Condens. Matter **192**, 55 (1993)
24. V. Harikrishnan, P. Saravanan, R.E. Vizhi, D.R. Babu, V.T.P. Vinod, P. Kejzlar, M. Černík, J. Magn. Magn. Mater. **401**, 775–783 (2016)
25. A.M. Abakumov, M.D. Rossell, O.Y. Gutnikova, O.A. Drozhzhin, Chem. Mater. **20**, 4457 (2008)
26. M.V. Patrakeeve, E.B. Mitberg, I.A. Leonidov, V.L. Kozhevnikov, Solid State Ion. **139**, 325 (2001)
27. M.D. Rossell, A.M. Abakumov, Q.M. Ramasse, R. Erni, ACS Nano **7**, 3078 (2013)
28. G. Mörée, M. Leijon, Materials (2023). <https://doi.org/10.3390/ma16062422>
29. S. Huang, K. Zhu, J. Huang, J. Yang, J. Wang, Z. Fu, R. Peng, Y. Lu, Ceram. Int. **48**, 19963 (2022)
30. A. Bardal, R. Bredesen, J. Mater. Sci. **36**, 5357 (2001)

Publisher's Note Springer Nature remains neutral with regard to jurisdictional claims in published maps and institutional affiliations.

Springer Nature or its licensor (e.g. a society or other partner) holds exclusive rights to this article under a publishing agreement with the author(s) or other rightsholder(s); author self-archiving of the accepted manuscript version of this article is solely governed by the terms of such publishing agreement and applicable law.